H-2-solid-state NMR study of benzene-d(6) confined in mesoporous silica SBA-15

ARTICLE *in* THE JOURNAL OF PHYSICAL CHEMISTRY B · FEBRUARY 2002

Impact Factor: 3.3 · DOI: 10.1021/jp012391p

^{2}H-Solid-State NMR Study of Benzene-d_6 Confined in Mesoporous Silica SBA-15

E. Gedat,[†] A. Schreiber,[‡] J. Albrecht,[†] Th. Emmler,[†] I. Shenderovich,[†] G. H. Findenegg,[‡] H.-H. Limbach,[†] and G. Buntkowsky*[,†,§]

Institut für Chemie, Freie Universität Berlin, Takustrasse 3, 14195 Berlin, Germany, and Stranski-Laboratorium für Physikalische und Theoretische Chemie, Technische Universität Berlin, Strasse des 17. Juni 112, 10623 Berlin, Germany

Received: June 21, 2001; In Final Form: November 28, 2001

Benzene-d_6 confined in the hexagonal ordered cylindrical pores of mesoporous silica SBA-15 (pore diameter 8.0 nm) was studied by low-temperature ^{2}H-solid-state NMR spectroscopy in the temperature range between 236 and 19 K and compared to bulk benzene-d_6. The solid-state spectra of the bulk benzene-d_6 exhibit quadrupolar Pake patterns at high and low temperatures, and in the intermediate temperature regime the typical line shape changes caused by rotational jumps around the 6-fold axis. At all temperatures the benzene molecules are characterized by a single rotational correlation time. For benzene-d_6 confined in SBA-15, however, these exchange dominated line shapes are not found. At all temperatures below the freezing point the spectra of benzene in the silica show the coexistence of two states with temperature-dependent intensity ratios. This behavior is the result of a Gaussian distributions of activation energies for the rotational jumps inside the pores. For the solid I−solid II (fast 6-fold jump to slow 6-fold jump) transition the center of the distribution is at 40 K (6.0 kJ/mol) with a width of 19.5 K (2.9 kJ/mol). For the liquid−solid I (liquidlike to fast 6-fold jump) transition the center of the distribution is at 204 K (30.6 kJ/mol) and the width is 15 K (2.2 kJ/mol). From the pore volume and the filling factor, a thickness of four molecular layers of this surface phase is estimated.

1. Introduction

Mesoporous silica materials are characterized by pores with diameters in the range between 2 and 50 nm.[12] Due to this wide range of pore sizes they are very versatile molecular sieves. Moreover, they are interesting model systems for the study of surface−liquid and surface−solid interactions. A well-known example of this class of mesoporous silica materials is MCM-41,[3] which is characterized by a hexagonal pore array (see Figure 1b) with a narrow distribution of pore sizes. MCM-41 is synthesized employing cationic tensides C_nTAB (trimethylalkylammoniumbromide) as templating agent, which provides well ordered pores with adjustable pore diameters between 2 and 6 nm. A new type of this class of systems is the recently developed silica SBA-15.[48] SBA-15, which is studied in this work, has adjustable pore diameters in the range between 5 and 15 nm. It is synthesized employing the triblock-copolymer polyethylenepropylene as templating agent. Both silica materials have a very high degree of order of the pore structure in common. Their main difference is the greater pore size of SBA-15, due to the different preparation. Because of their relatively small pore diameters MCM-41 silica have smooth pore surfaces, while SBA-15 pore surfaces exhibit a considerable roughness, which is attributed to $(SiO_2)_n$ islands on the surface.[41] Owing to the high density of pores and the relatively small pore diameters these silica materials have extremely large inner surfaces, as compared to the volume of the individual particle. Their Brunauer, Emmett, Teller (BET) surface area is about 1000 m^2/g and the specific pore volume is ca. 1 cm^3/g. Because of their large surfaces, a system of a liquid guest phase confined in these pores is an ideal model for the study of solid−liquid interface properties.

Since the physical properties of their inner surfaces, such as, for example, the surface acidity, can be chemically modified[2,45] mesoporous silica materials are very promising candidates for catalytic applications. The core phase in the center of the pores might function as the transport channel and a suitably prepared surface might serve as the catalyst. For possible catalytic applications the study of transport phenomena in the silica channels is of great interest, because the guest molecules need efficient transport channels to and from the inner surfaces of the pores, such that they can react, and afterward leave the pores and thus the catalytic power of the silica material is closely related to the transport process of the guest molecules through the pores. The potential for catalytic application has triggered several recent studies of the dynamics of guest molecules in mesoporous silica.[1,14,17,20,23,26,31,34]

A direct consequence of the solid−liquid interaction at the pore surface is the perturbation of the three-dimensional ordering of the guest molecules during formation of crystal structures when freezing the guest phase. Figures 1c−f schematically display possible scenarios of the arrangement of guest molecules in the pores and the resulting surface and pore-volume phases. The molecules in the direct vicinity of the surface experience forces according to the surface material and geometry, which in general are not compatible to the crystal packing forces of the crystal lattice.[30] As a result, the molecules in the vicinity of

* To whom all correspondence should be sent. E-mail: bunt@chemie.fu-berlin.de. Fax: +49 30 838 55310.
† Institut für Chemie.
‡ Stranski-Laboratorium für Physikalische und Theoretische Chemie.
§ Present address: Laboratory of Chemical Physics, NIDDK, National Institutes of Health, Building 5, Bethesda, MD 20892.

10.1021/jp012391p CCC: $22.00
Published on Web 02/02/2002

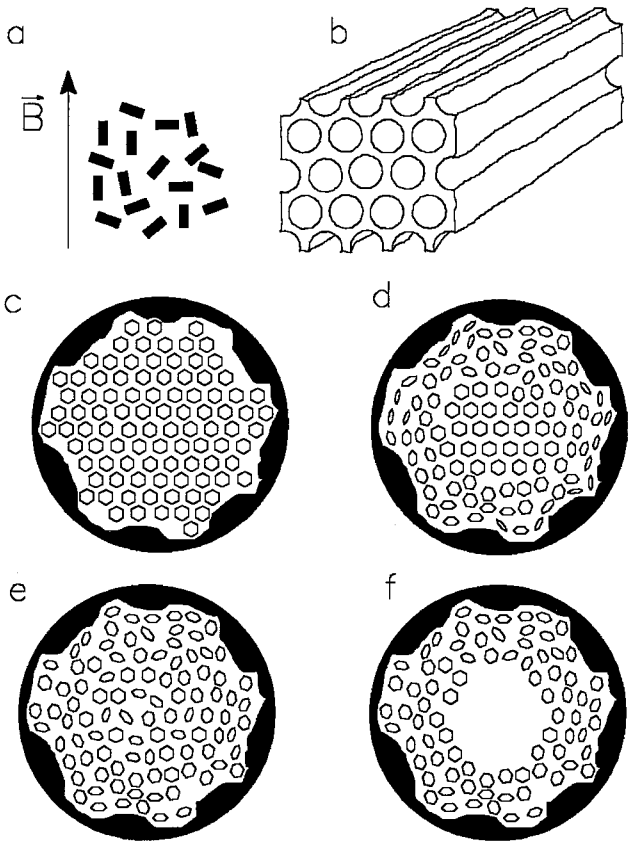

Figure 1. Models of the guest−host interaction of benzene in mesoporous silica of the SBA-15 type exhibiting cylindrical pores with a pore diameter of about 8 nm. (a) Distribution of microparticles in a magnetic field $\vec{B}$. (b) Hexagonal arrangement of cylindrical mesopores in a microparticle. (c) Sketch of a benzene guest assembly in a cylindrical pore with a rough surface in the absence of specific guest−host interactions. The packing of the benzene molecules is the same in the pores as in the bulk crystalline state. (d) The molecular arrangement changes gradually from the interface to the bulk, forming an ordered core phase. (e) The benzene molecules in the pore are completely unordered. (f) Arrangement of the benzene molecules such that the core in the middle of the pore is empty.

the surface will not easily align in the proper crystal positions and the formation of a crystal lattice is hindered or prohibited near the surface, leading to the formation of amorphous or pseudo liquid crystalline phases. In the vicinity of the surface, there will be vacancies and structural defects, which can enhance translational diffusion of the guest molecules and molecules in these surface phases will in general exhibit an increased rotational mobility at lower temperatures, as compared to the molecules in the crystalline phases. The dynamic behavior of molecules in this surface phase is expected to be dominated by the solid−liquid interaction. For large pore diameters they can form an additional inner pore volume phase which is expected to have similar properties such as the bulk phase. Note that such features are quite common for example in protein water solutions, where a phase of nonfreezable water in the hydration shell of the protein coexists with a phase of freezable bulk water.[6−8,22,27−29]

In our study we focus on the rotational properties of the molecules in the inner surface phase. We employ benzene-d_6 as a probe for monitoring the different rotational states by ^{2}H solid-state NMR spectroscopy, employing the well-known solid-state NMR spectra of bulk benzene[35,40] as a reference. If the correlation times of the different rotational motions are on the time scale of ^{2}H NMR, the mobility of benzene-d_6 can be directly monitored by ^{2}H NMR line shape analysis. The line shapes of the ^{2}H NMR spectra reveal the motional averaging of the quadrupolar coupling tensor,[4,46] which acts as a sensor for the state of ordering of the benzene. In bulk benzene three states with different kinds of rotational motion can be distinguished by ^{2}H NMR, namely, a liquid state and two solid states: The first (liquidlike) state corresponds to fast isotropic rotational motions of the benzene molecule. The second (solid I) state is an anisotropic rotational jump diffusion around the 6-fold axis. The third (solid II) state is the fully frozen state, where no rotational motion is present. In the region of the solid I−solid II transition, where the rate of the 60° jump is comparable to quadrupolar frequencies, typical motion-induced deviations from the common Pake pattern line shape are observed. These line shapes were reported by Vold et al.[35] for bulk benzene-d_6 and for benzene-d_6 confined in the cages of the cyclamer 1,3-cyclohexanedione. From the properties of bulk benzene it is evident that also in the silica the fully frozen phase (solid II) is expected at temperatures well below 100 K. For glass like systems of benzene however, a different behavior has been found.[40] Here a broad distribution of correlation times of the 6-fold jump motion renders the spectra corresponding to the intermediate (solid I−solid II) invisible. This leads to spectra, which are a weighted superposition of molecules rotating slow on the NMR time scale with solid-II-like spectra and molecules rotation fast on the NMR scale with solid-I-like spectra.

The dynamic range of motions detectable in the ^{2}H NMR spin−echo experiment is limited by the resolution and the sensitivity obtainable in the latter. This range could be enhanced on the low-frequency side by the technique of Geil et al.,[19] who recently showed that the regime of ultraslow motions can by analyzed in the time domain, employing ^{2}H-NMR-stimulated echoes, and on the high-frequency side by ^{2}H NMR spin lattice relaxation measurements as discussed by Rössler et al.[36]

The rest of the paper is organized as follows: First, the Experimental Section gives a short introduction into the basics of ^{2}H NMR line shape theory, describes the synthesis of the SBA-15 material, the NMR sample preparation, and our low-temperature ^{2}H NMR setup. Then the characterization of the material by X-ray diffraction and gas adsorption and the results of the experimental low-temperature ^{2}H NMR study of bulk benzene-d_6, and benzene-d_6 as guest molecule in the mesoporous silica SBA-15 are presented, discussed, and finally summarized.

2. Experimental Section

2.1. ^{2}H NMR Powder Spectra. The basic theory of solid state ^{2}H NMR is well-known[42,38] and only briefly summarized here.

The leading interaction in ^{2}H-solid-state NMR is the ^{2}H quadrupolar interaction. In the usual high field approximation, the first-order quadrupolar interaction is characterized by the Hamiltonian:

$$\hat{H}_Q = 2\pi\nu_Q(\vartheta,\varphi)\left(\hat{I}_z^{\,2} - \frac{2}{3}\right) \tag{1}$$

where the orientation dependent resonance frequencies ν_Q of the two transitions are given as (η, asymmetry parameter; and Q_{zz}, strength of the quadrupolar interaction):

$$\nu_Q(\vartheta,\varphi) = \pm\frac{3}{4}\frac{eQeq}{\hbar}(1/2)(3\cos^2\vartheta - 1 - \eta\sin^2\vartheta\cos 2\varphi)$$

$$= Q_{zz}\frac{1}{2}(3\cos^2\vartheta - 1 - \eta\sin^2\vartheta\cos 2\varphi) \tag{2}$$

While in single crystals, only two lines at $\pm\nu_Q$ are observable; in a nonoriented powder sample, the average over all possible orientations has to be calculated. Due to the axial symmetry of the magnetic field, it is sufficient to integrate over two angles (ϑ,φ), only. Assuming for simplicity that the transversal relaxation time T_2 is orientational independent, the spectra can be calculated as a superposition of simple Lorentzians:

$$I(\nu) = \int_0^{\pi} \mathrm{d}\vartheta \sin\vartheta \int_0^{2\pi} \mathrm{d}\varphi \left(\frac{T_2}{1 + 4\pi^2 T_2 (\nu - \nu_Q(\vartheta,\varphi))^2} + \frac{T_2}{1 + 4\pi^2 T_2 (\nu + \nu_Q(\vartheta,\varphi))^2} \right) \quad (3)$$

The quadrupolar coupling constant $Q_{cc} = {}^4/_3 Q_{zz}$ is a measure for the strength of the quadrupolar interaction. For rigid benzene (solid II), a practically axial symmetric quadrupolar tensor with $\eta < 0.05$ and a value of $Q_{zz} \cong 140$ kHz is found.[21,32,46] Because of the large spectral width, the ^{2}H NMR spectra are measured with the solid echo sequence $[90°_y - \tau - 90°_x - \tau - \langle \hat{I}_x \rangle]$. If the molecule undergoes fast reorientations the value of the quadrupolar tensor and thus also the quadrupolar coupling in general are changed, depending on the type and speed of the motion.[4] If the motions are fast on the NMR time scale, a relatively simple scenario is found: fast isotropic reorientations of the benzene molecule, as for example, in liquid benzene, cause a complete averaging of the quadrupolar tensor ($Q_{zz}^{iso} = 0$). Anisotropic rotations or rotational jump diffusions around the C_6-axis reduce the value of Q_{zz} to $Q_{zz}^{rot} = {}^1/_2 Q_{zz}$. In these situations the normalized line shape of the solid echo spectrum is identical to the FID spectrum. This is no longer the case if the correlation time of the motion is on the NMR time scale. Here, the line shape of the solid echo spectra becomes a function of the pulse spacing τ and has to be calculated by standard NMR methods.[38]

2.2. Preparation of the Mesoporous Silica SBA-15. The silica was prepared according to the procedure of Zhao et al.[48] employing Pluronic P103 ($EO_{17}-PO_{55}-EO_{17}$, EO = poly(ethylene oxide), and PO = poly(propylene oxide)), (BASF, Mt. Olive, NJ) as templating agent. Eight grams of P103 was dissolved in 480 mL of distilled water, 26 mL of 97% H_2SO_4 was added to the solution, then 18.4 mL of TEOS (tetraethoxysilane) was added under stirring at a temperature of 40 °C. The solution was first kept at 40 °C for 5 h and then at 108 °C for another 24 h. After this the product was rinsed with deionized water and calcined at 550 °C.

2.3. NMR Samples. Two different samples were studied, namely, the reference sample of bulk benzene-d_6, and a sample of the mesoporous silica SBA-15 loaded with benzene-d_6. The samples were filled into standard 5 mm NMR glass tubes, put on a vacuum line (200 mbar), frozen in liquid nitrogen, and flame sealed. For the silica/benzene-d_6 sample, 53.2 mg of SBA-15 were filled into the sample tube and tempered at 160 °C at 1×10^{-4} mbar for half an hour to remove any moisture and gases from the pores and clean the inner surfaces. From the specific pore volume of SBA-15 (see section 3.1), we estimated the total pore volume of this sample to 51.1 μL. To ensure that there is no extraporous benzene in the sample we loaded the pores with nominally 85% pore volume of liquid. Thus, 43.5 μL of benzene-d_6 99.6% (Aldrich) were added, which correspond to 41.3 mg of benzene. The reference sample of bulk-benzene contains approximately 50 mg benzene-d_6. A second similarly prepared sample was characterized by DSC, employing a cooling rate of 3K/min.

2.4. Low-Temperature ^{2}H NMR. A detailed discussion of our home-built three channel NMR spectrometer has been given recently.[10,44] Here, only some salient features are reproduced. All experiments were performed at a field of 6.98 T, corresponding to a ^{2}H resonance frequency of 45.7 MHz on a standard Oxford wide bore magnet (89 mm) equipped with a room-temperature shim unit. For the ^{2}H channel a 2 kW class AB amplifier from AMT equipped with an RF-blanking for suppressing the noise during data acquisition was employed. The RF was fed through a crossed diode duplexer, connected to the detection preamplifier and through the filters into the probe. Typical ^{2}H pulse width was 3.0 μs corresponding to 83 kHz B_1 field in frequency units.

All experiments were performed using a home-built 5 mm ^{2}H NMR probe. The probe is placed in a dynamic Oxford CF1200 helium flow cryostat. The sample temperature was controlled employing an Oxford ITC 503 temperature controller. During cooling and before and after data acquisition the sample temperature was directly controlled via a Cernox sensor placed in the direct vicinity of the sample. This temperature was used to calibrate the readings of a second CGR-1-1000 sensor, which is part of the cryostat. During data acquisition, the first sensor was disconnected from the ITC 503 and grounded to protect the ITC from the RF and to avoid distortions of the signal. Because of the high sensitivity of the ^{2}H NMR line shapes of both bulk and guest benzene-d_6 on the temperature, we carefully monitored the stabilization and equilibration of the temperature, allowing stabilization times up to several hours at each temperature before performing the NMR experiment.

All spectra were recorded using the solid echo technique, with an echo spacing of 30 μs and a full 32-step phase cycle. Before Fourier transformation, the echo-signal was phase corrected and the imaginary part zeroed to give fully symmetric spectra. The repetition times of the bulk benzene measurements were chosen according to Boden et al.,[5] using recycle delays from 3 s (high temperature) up to 120 s (lowest temperature). The number of accumulations was between 512 and 2048 scans per spectrum, with the exception of the bulk benzene spectra in the region of the solid I−solid II transition, where the echo amplitude is drastically reduced by the jump processes. Here, 22528 scans were recorded. For the measurements of the benzene guests in the silica pores, we had to ensure that the complete magnetization of all benzene molecules was fully relaxed and a quantitative evaluation of the concentrations of the molecules in the different rotational states is possible (see below). Therefore, several test spectra with different recycle delays were measured at each temperature; from these the optimal recycle time was determined, which was used for measuring the final spectrum.

For the interpretation of the ^{2}H NMR solid echo spectra of benzene-d_6 in the pores of SBA-15, the temperature-dependent spectra of the bulk benzene in the solid state are necessary as reference. In principle we could have used the temperature dependent ^{2}H NMR spectra of benzene-d_6, measured by Vold et al.[35] However, they employed relatively long echo delays of $\tau = 40$ μs and $\tau = 100$ μs. For better sensitivity we chose a shorter echo delay of $\tau = 30$ μs. Since the line shape in the intermediate exchange regime depends on the value of the echo delay in the solid echo sequence, the bulk benzene spectra had to be recorded with $\tau = 30\mu$s as a prerequisite for the interpretation of the data.

2.5. Data Evaluation. The echo spectra of benzene-d_6 in the fast and slow exchange regime were simulated using eq 3, employing a laboratory written Matlab program. Instead of numerically performing the powder integration, the faster

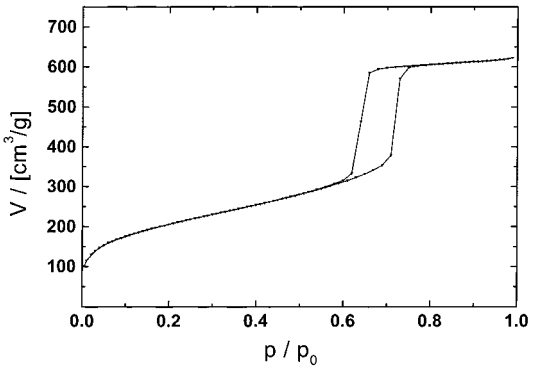

Figure 2. Nitrogen isotherm of the silica SBA-15, measured at standard temperature and pressure.

analytical expression of the powder pattern in terms of elliptic integrals[33] was used to calculate the line shape for zero width. The ^{2}H NMR echo spectra of the benzene in the intermediate exchange regime were simulated by a self-written Matlab routine using a Liouville formalism of the exchange process. For the powder integration over the polar angles (eq 3) an optimized angle set with 3554 angles was used.[11,13,47] The latter program was tested by reproducing the calculations shown in ref 35. Effects of the finite pulse power were taken into account using the formula given in.[38] The resulting Pake spectra were numerically convoluted with a Lorentzian by Fourier transformation into the time domain, multiplication with a decaying exponential function and transformation back into the frequency domain. In the SBA-15 sample, where two different subspectra are present (see results), the relative intensities of different spectral contributions were calculated from the integrals over the lines of the corresponding subspectra.

3. Results and Discussion

3.1. X-ray and Gas Adsorption. The mesoporous silica material SBA-15 was characterized by X-ray diffraction (Kratky camera, Cu Kα) and nitrogen adsorption (Gemini 2375, Micromeritics). The X-ray exhibits five diffraction peaks, which show that the silica is ordered in a two-dimensional hexagonal lattice with a lattice constant of $d_{100} = 8.68$ nm. This value corresponds to a pore to pore distance of $a_0 = 10.2$ nm. The pore diameter of 8.0 nm is determined from the adsorption branch of the nitrogen isotherm (Figure 2) employing the Dollimore and Heal formalism.[16] The pore volume and the specific BET surface area, as determined from the N_2 gas adsorption isotherm, are 720 m^2/g and 0.96 cm^3/g, respectively. A more detailed characterization of the SBA-15 material is given elsewhere.[39]

3.2. ^{2}H NMR Spectra of Bulk Benzene. Figure 3 displays the superposition of the experimental and simulated ^{2}H NMR spectra of bulk benzene in the temperature range between 206.6 and 88.4 K. The values of the quadrupolar interaction Q_{zz}, the asymmetry parameter η, and the jump rate k obtained from the simulation of the spectra, are collected in Table 1. The high-temperature spectrum at 206.6 K shows the solid I spectrum of bulk benzene-d_6 with a strength of the quadrupolar interaction of $Q_{zz}^{rot} = Q_{zz}/2 = 67.75$ kHz. It represents the fast jump limit (high-temperature limit). In the temperature region between 130.2 and 107.0 K, the jump rate is comparable to the NMR time scale and the typical effects on the line shape of the solid echo spectra[43] are visible, as discussed by Vold et al. for benzene-d_6.[35] At 88.4 K the slow jump limit (low-temperature limit) is reached with the solid II spectrum with

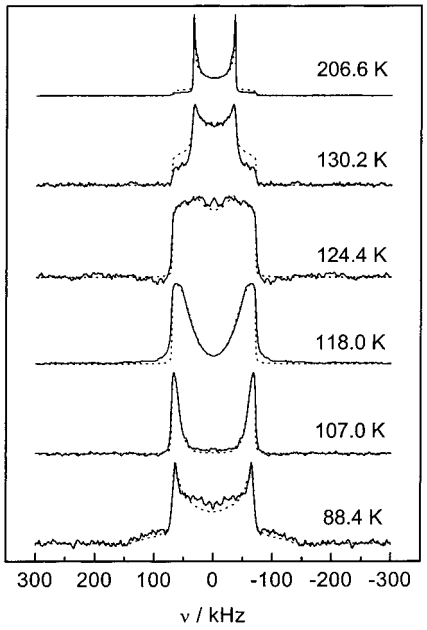

Figure 3. ^{2}H NMR spectra (—) and simulations (· ·) of bulk benzene-d_6 at various temperatures. In the temperature range of the transition from the solid I state (206.6 K) with a narrow Pake pattern ($Q_{zz} \cong 70$ kHz) to the solid II state (88.4 K) with a broad Pake pattern ($Q_{zz} \cong 140$ kHz) the rotational jump around the 6-fold axis causes strong deviations from the Pake line shape. The small negative intensities in the experimental spectrum at 124.4 K are noise. The simulations used included finite pulse effects.

TABLE 1: Fit Parameters of the ^{2}H NMR Spectra of Bulk Benzene-d_6 at Different Temperatures[a]

	T/K					
	88.4	107.0	118.0	124.4	130.2	206.6
Q_{zz}/kHz	133.0	136.5	136.0	136.0	136.0	135.5
η	0.03	0.04	0.04	0.04	0.04	0.01
k/s^{-1}	2.2k	100k	550k	1700k	4100k	1.8e6k

[a] The echo delay is $\tau = 30\ \mu$s. Listed are the quadrupolar interaction Q_{zz}, the asymmetry parameter η, and the exchange rate k. From the fits the errors are estimated to $\Delta Q_{zz} = \pm 0.5$ kHz and $\Delta\eta = \pm 0.01$.

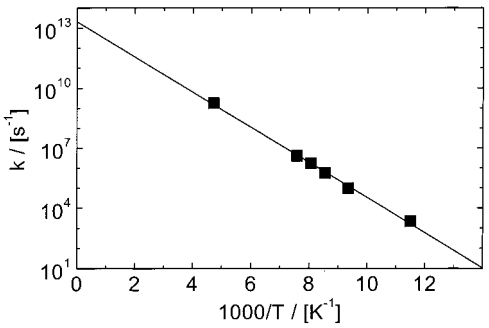

Figure 4. Arrhenius fit of the temperature-dependent jump rates of bulk benzene-d_6. The fit yields an activation energy of $E_a = 16.8$ kJ/mol and a preexponential factor of $k_0 = 2.0 \times 10^{13}$ s^{-1}.

$Q_{zz} = 133$ kHz. Figure 4 displays the rate constants of the 60° jumps around the molecular axis as a function of the inverse temperature. The data exhibit a typical thermally activated Arrhenius ($k = k_0\exp(E_a/RT)$) behavior. From the corresponding fit, a preexponential factor of $k_0 = 2.0 \times 10^{13}$ s^{-1} and an activation energy of $E_a = 16.8$ kJ/mol are determined. These values are in good agreement with the values determined by Vold et al.:[35] $k_0 = 2.0 \times 10^{13}$ s^{-1} and $E_a = 16.5$ kJ/mol.

TABLE 2: Fit Parameters of the ^{2}H NMR Spectra of Benzene-d_6 Confined in the Mesoporous Silica SBA-15 at Various Temperatures[a]

		T/K									
		236.1	204.8	187.4	154.3	120.9	92.5	75.5	51.8	31.1	19.0
L	rel int	1.000	0.501	0.127	0.002						
S−I	Q_{zz}^{rot}/kHz		69.8	69.3	68.7	69.8	70.1	70.0	71.3	71.0	71.5
	η		0.02	0.02	0.01	0.01	0.00	0.01	0.00	0.00	0.02
	rel int		0.499	0.873	0.998	0.999	0.995	0.984	0.695	0.342	0.127
S−II	Q_{zz}/kHz					(138.3)	(138.3)	(136.3)	138.2	135.8	135.7
	η					(0.05)	(0.05)	(0.05)	0.04	0.05	0.04
	rel int					0.001	0.005	0.016	0.305	0.658	0.873

[a] Listed are the quadrupolar interaction Q_{zz}, the asymmetry parameter η, and the relative (integral-) intensities (rel int) of the corresponding states. From the fits the errors are estimated to $\Delta Q_{zz} = \pm 1$ kHz and $\Delta\eta = \pm 0.0$. Values in parentheses represent estimations due to very low intensity. L, S−I, and S−II are the liquidlike, the solid-I-like, and the solid-II-like molecules.

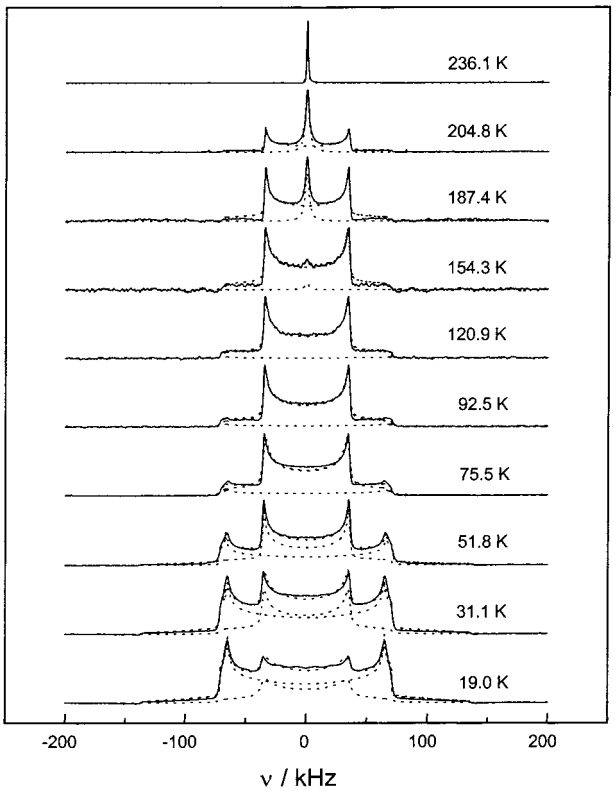

Figure 5. ^{2}H NMR spectra (—) and simulations (· ·) of benzene-d_6 confined in the pores of the mesoporous silica SBA-15 for various temperatures. Except for the liquid spectrum (236.1 K), the two dashed subspectra for each temperature represent the corresponding liquid/solid I/solid II states. The third dashed line is the sum of both subspectra.

3.3. ^{2}H NMR Spectra of Benzene Confined in SBA-15. The experimental and simulated ^{2}H NMR spectra of benzene-d_6 confined in the pores of the mesoporous silica SBA-15 in the temperature range between 19.1 and 236.1 K are shown in Figure 5. The quadrupolar coupling constants Q_{zz} and the asymmetry parameters η obtained from the simulation of the spectra are collected in Table 2, together with the relative intensities of the three different states: liquidlike, solid I, and solid II. The intensities are derived by calculating the integrals of the subspectra. Even at 236.1 K there is one single narrow line of the liquidlike benzene like molecules, indicating a lowering of the freezing point of the isotropic benzene rotation in the pores of at least 43.9 K. The absence of a solid-I-like Pake component at this temperature shows that there is no measurable amount of benzene outside the pores and all benzene is confined inside the pores, as intended by the sample preparation. The spectrum measured at 204.8 K consists of a superposition of two lines: a narrow central line stemming from liquidlike benzene and a broad Pake line with a width of $Q_{zz} \cong$ 70 kHz, similar to the solid I phase of bulk benzene. Upon lowering the temperature of the sample the relative intensities of the two lines change gradually until finally at 120.9 K the liquidlike line has completely disappeared. Upon further cooling a second Pake like component with a line width of $Q_{zz} \cong$ 138 kHz, similar to the solid II phase, appears in the spectrum, which finally dominates the spectra at 31.1 K and below. However, even in the spectrum measured at 19.0 K both Pake-like components are still visible in the spectrum.

3.4. Discussion. As shown above, the ^{2}H NMR spectra of benzene-d_6 in SBA-15 are a superposition of two different components. In both components we note the absence of any signals typical for an intermediate rotational exchange regime in the ^{2}H NMR spectra, i.e., spectra with the line shape of bulk benzene at temperatures between 100−130K. Here, the benzene molecules are found in two separate Pake subspectra of solid I and solid II type with temperature dependent relative concentrations. At higher temperatures most molecules are in the solid-I-like line. Upon lowering of the temperature, more and more of the benzene molecules are found in the solid-II-like line. In particular there is no longer a well defined phase transition temperature for the freezing of the rotational motion. This temperature dependence of the benzene spectra in SBA-15 is pronouncedly different from the behavior of benzene dissolved in the cyclamer 1,3-cyclohexanedione studied by Vold et al. It resembles closely the behavior of benzene molecules in frozen liquid-crystalline polysiloxane presented by Schulz et al.[40] This temperature dependence is characteristic for a broad distribution of correlation times of the rotational reorientation of the benzene molecules, caused by a distribution of activation energies. In other words, it is a glasslike behavior, which results from the disorder that is induced by the solid−liquid interaction of the pore walls with the guest molecules. As a consequence, at any temperature only a small part of benzene molecules is in the intermediate regime, while the majority is either in the fast or slow regime. Therefore, only the latter are visible in the spectra. Because the subspectra are not attenuated by the echo experiments they are a direct measure for the number of molecules in the fast, respectively slow rotating state. Typical examples of these scenarios are polymer glasses, as discussed by Rössler et al.[36] They describe a procedure for the evaluation of the distribution of correlation times. They assume that the distribution of activation energies $p(E,T)$ does not vary significantly with temperature and conclude that the relative amount of molecules in each state (liquidlike,

solid I-like, solid II-like) is an integral measure of the distribution function of the activation energies. Since always only two subspectra are visible in the spectra, the relative concentrations are related via

$$c_A(T) = \int_0^{E^*} p(E,T)\,dE$$

$$c_B(T) = \int_{E^*}^{\infty} p(E,T)\,dE$$

$$= 1 - c_A(T) \qquad (4)$$

to the temperature, where $c_A(T)$ denotes the slow and $c_B(T)$ denotes the fast exchanging fraction of molecules. Here, $E^*(T)$ is a temperature-dependent activation energy characteristic for the intermediate exchange regime. For a Gaussian distribution of activation energies,[36] they rewrite eq 4 to (E_0, center of gravity; and ΔE, width of the Gaussian distribution):

$$c_A(T) = \int_0^{E^*(T)} \frac{1}{\sqrt{2\pi\Delta E^2}} \exp\left(-\frac{(E-E_0)^2}{2\Delta E^2}\right) dE \qquad (5)$$

Calculating the derivative of $c_A(T)$, the distribution of activation energies is obtained:

$$\frac{d}{dT} c_A(T) = \frac{1}{\sqrt{2\pi}\Delta T} \exp\left(-\frac{(T-T_0)^2}{2\Delta T^2}\right)$$

$$= g(E) \qquad (6)$$

Since we are measuring the intensity ratios, i.e., the relative concentration of fast and slow rotating molecules, we have to integrate this expression over the temperature.

$$c_A(T) = \int_0^T \frac{1}{\sqrt{2\pi\Delta T^2}} \exp\left(-\frac{(T-T_0)^2}{2\Delta T^2}\right) dT$$

$$= \frac{1}{2}\mathrm{erf}\left(\frac{1}{\sqrt{2}\Delta T}(T-T_0)\right) + \frac{1}{2}\mathrm{erf}\left(\frac{1}{\sqrt{2}\Delta T}T_0\right) \qquad (7)$$

where erf(x) is the Gaussian error function.

The conversion between temperature and energy is done assuming an Arrhenius dependence between the characteristic activation energy, the temperature, and the correlation times of the jump process:

$$E(T) = \ln\left(\frac{\tau(T)}{\tau_\infty}\right) kT =: \alpha T \qquad \text{with } \alpha = \ln\left(\frac{\tau(T)}{\tau_\infty}\right) k \quad (8)$$

For the evaluation of the experimental data the value of α has to be estimated, which implies the estimation of the values of the correlation times $\tau(T^*)$ and τ_∞. Since only the logarithm of there ratio is used, we can assume the value of bulk benzene obtained from Figure 4, i.e., $\tau_\infty = 5 \times 10^{-14}$ s for the latter. For $\tau(T^*)$ we choose a value which is in the middle of the intermediate exchange regime, namely, $\tau(T^*) = 3 \times 10^{-6}$ s. With these values the following relation between E and T is found:

$$E = \ln\left(\frac{\tau(T^*)}{\tau_\infty}\right) kT = 17.9kT \qquad (9)$$

For the coexistence of both slow and fast-rotating molecules in the solid I to solid II transition this model is the unique explanation. For the transition from liquidlike to solid-I-like spectra however, an alternative explanation was found by Roessler et al.[36] They studied the dependence of the phase transition on the concentration of guest molecules in a polymer matrix and found that this dependence is in contradiction to a distribution of activation energies. Instead they conclude that the glass dynamics is broadened as the consequence of a distribution of different sites inside the polymer matrix, which also results in a superposition of a liquidlike and a motionally narrowed Pake spectrum. Such a broadened glass transition cannot be excluded in our system and thus this is also a possible interpretation of our experimental results. However, in contrast to the polymer system studied in ref 36, there are three main differences in our system, which are in favor of a distribution of activation energies as the origin of the superposition of solid-I-like and liquidlike spectrum:

1. DSC measurements (Figure 8) show the phase transition temperature for the translational motion ("freezing") at 233K, which is ca. 30K higher as the "freezing" temperature of the liquidlike reorientations (204K).

2. The calculated activation energy of the isotropic rotations with a value of 30.6 kJ/mol is ca. a factor of 5 larger than typical reorientation energies of molecules in liquids.

3. The geometry of the benzene-molecules on the surface of the silica is less inhomogeneous than the various sites inside a disordered polymer-matrix.

These factors can be interpreted in the following way: after the freezing of the translational degrees of freedom of the benzene molecules, the individual molecules still have a relatively large free space, which allows isotropic reorientations of the benzene molecules. However there is already considerable "friction" for the reorientation of the 6-fold axis, which is visible in the high activation energy of 30.6 kJ/mol. Because of the roughness of the surface and the distance of the benzene molecules from the surface there is a distribution of environments for the benzene molecules, which causes the distribution of activation energies, visible in the ^{2}H NMR spectra.

Assuming that both transitions are describable as distributions of activation energies, the relative amounts $c_A(T)$ and $c_B(T)$ can be determined from the integral intensity of the corresponding experimental subspectra in Figure 5. The data are collected in Table 2, and plotted in Figure 6, together with a fit of eq 7 to the data for both transitions. Figure 7 finally displays the derivatives of the fitted curves, i.e., the Gaussian distributions of phase transition temperatures and activation energies, respectively. From these curves the centers of gravity $T_0(E_0)$ and the widths of the distributions $\Delta T(\Delta E)$ are determined. The resulting values are $T_0^{(h)} = 204$ K ($E_0^{(h)} = 30.6$ kJ/mol) for the

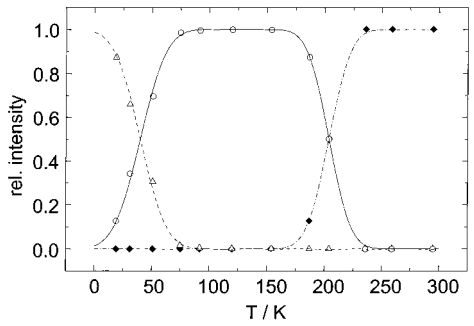

Figure 6. Relative intensities of the three rotational states liquid (◆), solid I (○), and solid II (△) of benzene in the pores of the mesoporous silica SBA-15 as a function of temperature. The simulated relative intensities of the liquid state (· —), the solid I state (—), and the solid II state (- -) are calculated with eq 7.

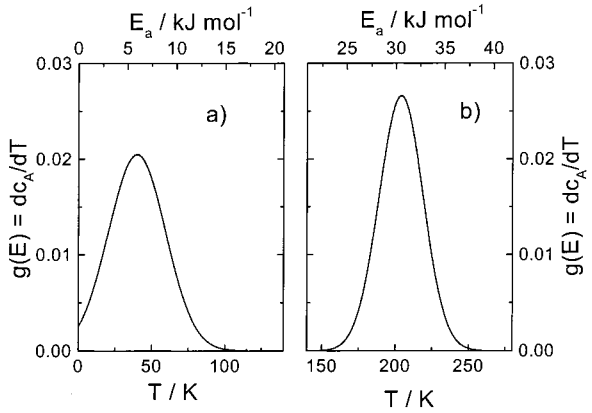

Figure 7. Distribution of the phase transition temperatures (and activation energies) for 60° jump motion of benzene-d_6 in SBA-15 as calculated with eq 8: (a) solid I−solid II transition and (b) liquid−solid I transition.

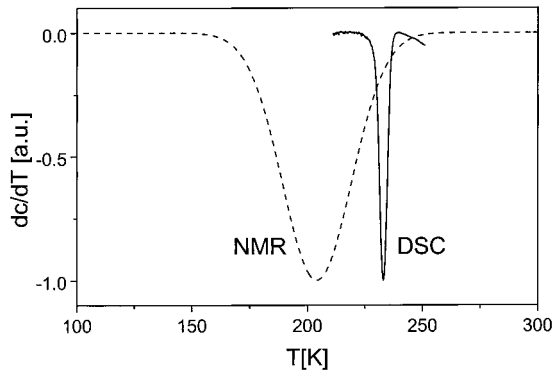

Figure 8. Comparison of the DSC-curve of the freezing of the translational degrees of freedom of benzene inside the mesopores with the NMR curve of the freezing of the isotropic rotations of benzene inside the mesopores. Note that there is a difference of 29 K between the two freezing points.

liquid−solid I transition and $T_0^{(l)} = 40$ K ($E_0^{(l)} = 6.0$ kJ/mol) for the solid I−solid II transition. The widths of the distributions are $\Delta T^{(h)}$=15 K ($\Delta E^{(h)} = 2.2$ kJ/mol) and $\Delta T^{(l)} = 19.5$K ($\Delta E^{(l)} = 2.9$ kJ/mol), respectively.

These differences to the behavior of bulk benzene are the result of the interaction of the benzene molecules with the silica surface. The surface induces a geometric arrangement of the benzene molecules, which is not compatible to the crystal lattice of bulk benzene. As a result a surface phase is established. There are three possible structures of the surface phase, which can account for the observed behavior: (i) the surface phase is a purely amorphous phase with no long range order, similar to a glass (Figure 1e); (ii) the surface phase consists of ordered layers of benzene molecules and the orientation of the molecules and the corresponding activation energies in the layers changes gradually from layer to layer, similar to a cholesteric liquid crystal and the distribution of activation energies is the distribution of the activation energies of each layer; (iii) the surface phase changes gradually from a purely disordered to a fully ordered phase (Figure 1d). Due to the roughness of the surface and the broad distribution of activation energies the second possibility can be excluded, leaving the model of full disorder or the gradual change from order to disorder. On one hand the very broad distribution of activation energies for the rotational motion, which is similar to the results measured in glasses,[9,25,37] suggests the first explanation as the more plausible one. On the other hand the relatively narrow DSC peak is in favor of an ordered system regarding the translational degrees of freedom, which would exclude a "true" glass. From this it follows that the benzene molecules in these inner surface layers neither behave like a "true" glass nor like a crystal, but like a strongly disordered pore solid[24] which partially resembles a glass and partially a crystal.

An interesting question is, how this glasslike behavior depends on the pore diameter. For large pore diameters which are completely filled one clearly expects a crystalline structure of the inner core phase, which has properties similar to the bulk phases of benzene. If the pores are not completely filled, in addition differences in the interaction strength between benzene molecules and between molecules and the surface have to be taken into account. Depending on these interactions two limiting scenarios are possible for partially filled pores, namely, (i) the guest phase occupies the whole cross section of the pores (Figure 1d,e), but leaves a part of the pores completely empty; (ii) the filling of the pores grows from the surface toward the center of the pore, leaving an empty cylinder in the center of the pore (Figure 1f). From the present data it is not possible to decide between these alternatives. A possible way to distinguish between these scenarios are measurements of translational diffusion of the benzene molecules inside the pores, which are beyond the scope of this paper. In the case of complete filling of the pores the benzene-air surfaces would act as boundaries for the translational diffusion of the benzene molecules, which should be visible in the diffusion measurements, similar to the diffusion of pyridine molecules in mesoporous silica.[18]

The thickness of the surface phase, which is a measure of the depth of the surface−liquid interaction, depends on the scenario. In the first case the depth is simply the pore radius. In the second case the thickness of the surface phase can be calculated from the pore diameter and the filling factor (85%) of the pores as ($d = r_{pore} - r_{core}$, h = height of the cylinder, V_{pore}, V_{core} = volumes of the inner and outer cylinder):

$$V_{pore} = \pi r_{pore}^2 h; \quad V_{core} = \pi r_{core}^2 h$$

$$\frac{V_{core}}{V_{pore}} = \frac{r_{core}^2}{r_{pore}^2} = x$$

$$d = (1 - \sqrt{x}) r_{pore} \qquad (10)$$

Employing the pore radius of $r_{pore} = 4.0$ nm and the relative volume of $x = 0.15$, a thickness of the adsorbed phase $d = 2.45$ nm is estimated. This value can be compared to typical benzene distances in the solid. Employing the X-ray of bulk benzene (space group *Pbca*, $a = 0.7460$, $b = 0.9666$, and $c = 0.7034$ nm; four molecules per unit cell[15]) a typical next-neighbor distance of 0.57 nm for bulk benzene is calculated. Assuming that the density in the inner surface phase is approximately the same as in bulk benzene, the surface phase has an average thickness of approximately 4.3 molecular layers of benzene.

Thus our results show that the interactions with the surface are transmitted over at least four molecular layers of benzene, preventing the establishment of an ordered benzene phase with bulklike properties. Since this disordered phase takes up already 85% of the pore volume, it is evident that much larger pore diameters are necessary to establish an inner core phase with bulklike properties. In such a system one would expect a bimodal distribution of activation energies with one sharp maximum for the inner core phase and the broad distribution of the disordered surface phase.

4. Conclusion

By careful selection of the pore diameter and preparation of the sample we were able to prepare a pure inner surface phase of benzene molecules as guests in the mesopores of SBA-15. There is a relatively narrow phase transition temperature distribution for the translational motion ("freezing") of the benzene molecules inside the pores. However, the benzene molecules in this inner surface phase exhibit a broad distribution of rotational correlation times for the 6-fold jump of the benzene molecules around their molecular symmetry axis. This distribution of correlation times can be attributed to a broad distribution of activation energies for the rotational motions. Assuming an Arrhenius relation between correlation times and activation energies and a Gaussian distribution of activation energies, it is possible to elucidate the centers of gravity and the widths of these activation energy distributions of the liquid−solid I and the solid I−solid II transitions from the experimental data.

Acknowledgment. This work was supported by the Deutsche Forschungsgemeinschaft in the framework of the Sonderforschungsbereich 448 "Mesoskopisch Strukturierte Verbundsysteme".

References and Notes

(1) Aknes, D. W.; Gjerdaker, L. *J. Mol. Struct.* **1999**, 27.
(2) Anwander, R.; Nagl, I.; Widenmayer, M.; Engelhardt, G.; Groeger, O.; Palm, C.; Röser, T. *J. Phys. Chem. B* **2000**, *104*, 3532.
(3) Beck, J. S.; Vartuli, J. C.; Roth, W. J.; Leonowicz, M. E.; Kresge, C. T.; Schmitt, K. D.; Chu, C. T.-W.; Olson, D. H.; Sheppard, E. W.; McCullen, S. B.; Higgins, J. B.; Schlenker, J. L. *J. Am. Chem. Soc.* **1992**, *114*, 10834.
(4) Boddenberg, B.; Grosse, R. *Z. Naturforsch.* **1986**, *41a*, 1361.
(5) Boden, N.; Clark, L. D.; Hanlon, S. M.; Mortimer, M. *Faraday Symp. Chem. Soc.* **1978**, 109.
(6) Bodurka, J.; Buntkowsky, G.; Gutsze, A.; Limbach, H.-H. *Appl. Spectrosc.* **1996**, *50*, 1421.
(7) Bodurka, J.; Buntkowsky, G.; Gutsze, A.; Limbach, H.-H. *Z. Naturforsch.* **1996**, *51c*, 81.
(8) Bodurka, J.; Gutsze, A.; Buntkowsky, G.; Limbach, H.-H. *Z. Chem. Phys.* **1995**, *190*, 99.
(9) Börner, K.; Diezemann, G.; Rössler, E.; Vieth, H. M. *Chem. Phys. Lett.* **1991**, *181*, 563.
(10) Buntkowsky, G.; Sack, I.; Limbach, H.-H.; Kling, B.; Fuhrhop, J. *J. Phys. Chem. B* **1997**, *101*, 11265.
(11) Cheng, V. B.; Suzukawa, H. H.; Wolfsberg, M. *J. Chem. Phys.* **1973**, *59*, 3992.
(12) Ciesla, U.; Schüth, F. *Microporous Mesoporous Mater.* **1999**, *27*, 131.
(13) Conroy, H. *J. Chem. Phys.* **1967**, *47*, 5307.
(14) Courivaud, F.; Hansen, E. W.; Kolboe, S.; Karlsson, A.; Stöcker, M. *Microporous Mesoporous Mater.* **2000**, *37*, 223.
(15) Cox, E. G.; Cruickshank, D. W. J.; Smith, J. A. S. *Proc. R. Soc. London Ser. A* **1958**, *247*, 1.
(16) Dollimore, D.; Heal, G. R. *J. Appl. Chem.* **1964**, *14*, 109.
(17) Edgar, M.; Schubert, M.; Limbach, H. H.; Göltner, C. G. *Ber. Bunsen-Ges. Phys. Chem.* **1997**, *101*, 1769.
(18) Gedat, E.; Schreiber, A.; Findenegg, G.; Shenderovich, I.; Limbach, H.-H.; Buntkowsky, G. *Magn. Res. Chem.* **2001**, *39*, 149.
(19) Geil, B.; Fujara, F.; Sillescu, H. *J. Magn. Res.* **1998**, *130*, 18.
(20) Gjerdaker, L.; Sorland, G. H.; Aknes, D. W. *Micro. Mesoporous Mater.* **1999**, *32*, 305.
(21) Grundke, V.; Boddenberg, B. *Mol. Phys.* **1993**, *79*, 1215.
(22) Gutsze, A.; Bodurka, J.; Olechnowicz, R.; Buntkowsky, G.; Limbach, H.-H. *Z. Naturforsch.* **1995**, *50c*, 410.
(23) Hansen, E. W.; Schmidt, R.; Stöcker, M.; Akporiaye, D. *Microporous Mater.* **1995**, *5*, 143.
(24) Jackson, C. L.; McKenna, G. B. *J. Chem. Phys.* **1990**, *93*, 9002.
(25) Jansen-Glaw, B.; Roessler, E.; Taupitz, M.; Vieth, H. M. *J. Chem. Phys.* **1989**, *90*, *12*, 6858.
(26) Jobic, H. *Phys. Chem. Chem. Phys.* **1999**, *1*, 525.
(27) Kimmich, R. *NMR Tomography Diffusometry Relaxometry*; Springer: Berlin, 1997.
(28) Kimmich, R.; Klammler, F.; Skirda, V. D.; Serebrennikova, I. A.; Maklakhov, A. I.; Fatkullin, N. *Appl. Magn. Res.* **1993**, *4*, 425.
(29) Kimmich, R.; Weber, H. W. *Phys. Rev. B* **1993**, *47*, 788.
(30) Kitaigorodski, A. I. *Molekülkristalle*; Akademie-Verlag: Berlin, 1979.
(31) Ladizhansky, V.; Hodes, G.; Vega, S. *J. Phys. Chem. B* **2000**, *104*, 1939.
(32) Mantsch, H. H.; Saito, H. S.; Smith, I. C. P. *Prog. NMR Spec.* **1977**, *11*, 211.
(33) Mehring, M. *High-Resolution NMR Spectroscopy in Solids*; Springer-Verlag: New York, 1983.
(34) Mel′nichenko, Y. B.; Schüller, J.; Richert, R.; Ewen, B.; Loong, C.-K. *J. Chem. Phys.* **1995**, *103*, 2016.
(35) Ok, J. H.; Vold, R. R.; Vold, R. L.; Etter, M. C. *J. Phys. Chem.* **1989**, *93*, 7618.
(36) Roessler, E.; Taupitz, M.; Börner, K.; Schulz, M.; Vieth, H. M. *J. Chem. Phys.* **1990**, *92*, 5847.
(37) Roessler, E.; Taupitz, M.; Vieth, H. M. *J. Phys. Chem.* **1990**, *94*, 6879.
(38) Schmidt-Rohr, K.; Spiess, H. W. *Multidimensional Solid State NMR and Polymers*; Academic Press: London, 1994.
(39) Schreiber, A.; Ketelsen, I.; Findenegg, G. H. *Phys. Chem. Chem. Phys.* **2001**, *3*, 1185.
(40) Schulz, M.; van der Est, A.; Rössler, E.; Kossmehl, G.; Vieth, H. M. *Macromolecules* **1991**, *24*, 5040.
(41) Shenderovich, I.; Schreiber, A.; Gedat, E.; Buntkowsky, G.; Golubev, N. S.; Findenegg, G. H.; Limbach, H. H. 2001. In preparation.
(42) Slichter, C. P. *Principles of Magnetic Resonance*, 3rd ed.; Springer-Verlag: New York, 1990.
(43) Spiess, H. W.; Sillescu, H. *J. Magn. Reson.* **1981**, *42*, 381.
(44) Wehrmann, F.; Fong, T.; Morris, R. H.; Limbach, H.-H.; Buntkowsky, G. *Phys. Chem. Chem. Phys.* **1999**, *1*, 4033.
(45) Whilton, N. T.; Berton, B.; Bronstein, L.; Hentze, H.-P.; Antonietti, M. *Adv. Mater.* **1999**, *11*, 1014.
(46) Xion, J.; Maciel, G. E. *J. Phys. Chem. B* **1999**, *103*, 5543.
(47) Zaremba, S. K. *Ann. Mater. Pura. Appl.* **1966**, *4*, 293.
(48) Zhao, D.; Feng, J.; Huo, Q.; Melosh, N.; Fredrickson, G. H.; Chmelka, B. F.; Stucky, G. D. *Science* **1998**, *279*, 548.